RSC Advances

PAPER

View Article Online
View Journal | View Issue

Cite this: *RSC Adv.*, 2026, **16**, 27994

Bio-degradable electrospun nanofibers encompassing dioxidovanadium benzimidazole compounds as potential drug delivery systems for diabetes mellitus

Sanam Maikoo,*[a] Mongezi Majebe,[a] Andile Khathi,[b] Allen Mambanda,[a] Bongeka Mshengu,[b] Lindokuhle Patience Mabuza,[b] Phikelelani Ngubane[b] and Irvin Noel Booysen *[a]

Insulin-mimetic organovanadium compounds: *cis*-[VO_2(Hpybz)(pybz)] (**1**) (Hpybz = 2-pyridyl-1*H*-benzimidazole) and *cis*-[VO_2(obz)py] (**2**) (Hobz = 2-hydroxyphenyl-1*H*-benzimidazole and py = pyridine) were encapsulated in biodegradable electrospun nanofibres (ENFs) comprising polyvinyl alcohol (PVA) and chitosan (CS). Morphological features and elemental compositions of the unconjugated and metal complex-ENFs adducts were investigated *via* scanning electron microscopy (SEM) micrographs, which were accompanied by electron-dispersive X-ray (EDX) spectra. Solid-state infrared and powder X-ray diffraction spectral analysis showed that the metal complexes are largely confined within the nano-confined polymeric strands. Intracellular uptake studies revealed sustained vanadium uptake in Caco-2 cells, indicating improved intestinal support. Cell viability studies revealed no significant toxicity across the tested concentrations in HepG2 and C2C12 cells, whilst *in vitro* glucose utilization assays showed a noteworthy enhancement in cellular glucose uptake, consistent with insulin-mimetic activity. ENFs loaded with complex **1** showed superior glucose-lowering potential.

Received 25th February 2026
Accepted 1st June 2026

DOI: 10.1039/d6ra01655c

rsc.li/rsc-advances

Introduction

Type 2 diabetes mellitus (T2DM) is a life-threatening non-communicable disease that has shown an increasing prevalence worldwide.[1] Steady escalation in the annual T2DM-induced fatalities still occurs, even though intravenous injection of insulin remains the mainstream therapy while orally administered drug alternatives such as Metformin serve as secondary therapeutic treatments.[1,2] Among various prospective transition metal-based anti-diabetic drugs, some selected organovanadium compounds have emerged as promising metallo-drug candidates for T2DM.[3] The proposed mechanism of anti-diabetic activity of these vanadium compounds is largely based on their ability to inhibit protein tyrosine phosphatase 1B (PTP-1B) in the insulin signalling pathway.[4]

Oral drug administration is the preferred method for treating both non-infectious and transmissible diseases, including T2DM. In particular, the advantages of oral administration over traditional intravenous injections include patient convenience, providing facile drug administration with essentially no discomfort and minimal risk of cross-infection.[5] However, oral therapeutics are often accompanied by limitations such as low stability under acidic conditions of the stomach as well as poor aqueous solubility and adsorption through the stomach lining and membrane, leading to minimal bioavailability.

Nanomaterial-based drug delivery systems have demonstrated the ability to overcome many of the limitations of current oral antidiabetics, offering improved solubility, sustained drug release, and enhanced bioavailability.[6–9] In particular, electrospun nanofibers (ENFs) can act as guest-host systems where a pharmaceutical as a guest is typically included within the nano-confined polymer strands.[10] Furthermore, the drug-release kinetics of ENF-drug composites can be conveniently manipulated through alteration of the instrumental and solution parameters.[11,12]

In the present work, we present a series of Poly(vinyl alcohol)-Chitosan (PVA-CS) ENFs loaded with our previously reported vanadium heterocyclic compounds, *cis*-[VO_2(Hpybz)(pybz)] (**1**) (Hpybz = 2-pyridyl-1*H*-benzimidazole) and *cis*-[VO_2(obz)py] (**2**) (Hobz = 2-hydroxyphenyl-1*H*-benzimidazole and py = pyridine), see Fig. 1.[13–16] The '2 + 2' dioxidovanadium(v) benzimidazole compound **1** showed glucose-lowering capabilities in selected liver and skeletal muscle cell lines, while the diamagnetic mono-benzimidazole diamagnetic vanadium compound **2** exhibited conducive *in vivo* anti-diabetic

[a]*School of Agriculture and Science, University of KwaZulu-Natal, Pietermaritzburg, 3201, South Africa. E-mail: smaikoo7@gmail.com; booyseni@ukzn.ac.za*
[b]*School of Laboratory Medicine and Medical Sciences, University of KwaZulu-Natal, Durban, South Africa*

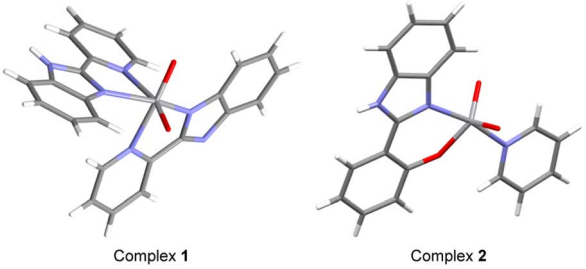

Fig. 1 Solid-state structures of **1** and **2**. Reproduced from Polyhedron, Irvin N. Booysen, Thulani Hlela, Thomas I.A. Gerber, Orde Q. Munro, Matthew P. Akerman, Novel vanadium compounds with 2-pyridylbenzimidazole, 79, 250–257, 2014 and Polyhedron, Irvin Noel Booysen, Thulani Hlela, Matthew Piers Akerman, Bheki Xulu, Mono- and polynuclear vanadium(IV) and -(V) compounds with 2-substituted phenyl/pyridyl heterocyclic chelates, 85, 144, 2015 with permission from Elsevier.

properties in a Streptozotocin (STZ)-diabetic rat model, accompanied by limited cytotoxicity Characteristically, these monomeric vanadium heterocyclic compounds act as pro-drugs which convert to vanadate that displays *in vitro* inhibitory PTP-1B enzyme activities.[17]

A bulk polymer blend of PVA and CS is a commonly preferred precursor for electrospinning biocompatible drug-delivery systems.[18,19] More specifically, PVA is a biodegradable, biocompatible synthetic polymer.[20] In addition, the blending of CS with PVA generally results in the nanofabrication of monodisperse PVA-CS ENFs with high mechanical strength. In addition, chitosan (CS) is one of the most naturally abundant polysaccharides, and its inherent biological relevance makes it well-suited for inclusion in hybrid materials for biomedical applications.[21] Herein, the surface morphologies and elemental compositions of the PVA-CS ENFs and their vanadium compound conjugated derivatives were scrutinized using Scanning electron microscopy with energy dispersive X-ray spectroscopy (SEM-EDX), while FT-IR spectroscopy and powder X-ray diffractometry (XRD) were used to characterize them. Furthermore, the drug release profiles and the percentage radical-scavenging activity of the complex-loaded electrospun nanofibers were measured using UV-Vis spectrophotometry. The drug loading and entrapment efficiency percentages were also established. In this drug-delivery design, the ENFs serve as drug-delivery frameworks for the encapsulated bioactive vanadium complexes. These ENFs are orally compatible and biodegradable, while ensuring controlled release of the vanadium complexes in the gastrointestinal (GI) tract, modulated by pH. Once released, the vanadium complexes are absorbed into the intestinal lining and, subsequently, into the bloodstream for antidiabetic control.

Experimental

Materials and methods

The organic precursors: 2-hydroxyphenyl-1*H*-benzimidazole and 2-pyridyl-1*H*-benzimidazole, as well as the metal precursor, NH_4VO_3, were purchased from Sigma-Aldrich. Analytical-grade solvents were obtained from Merck SA and used without further purification. Medium molecular weight chitosan, hydrolyzed poly(vinyl alcohol) (Mw: 89.000 to 98.000 g mol^{-1}, 99% hydrolyzed), high purity ascorbic acid, phosphate buffered saline tablets, Trizma hydrochloride, 2,2-diphenyl-1-picrylhydrazyl (DPPH), Dulbecco's Modified Eagle Medium (DMEM), fetal bovine serum, L-glutamine, penicillin/streptomycin solution, and sodium pyruvate were also purchased from Sigma-Aldrich. HepG2 liver, C2C12 skeletal muscle, and Caco-2 cell lines were obtained from Cellonex, South Africa. Solid-state infrared spectra were recorded on a Bruker Alpha II FTIR spectrometer equipped with an attenuated total reflectance (ATR) platinum Diamond 1 attachment. Spectrophotometric measurements were carried out using an Agilent Cary 60 spectrophotometer.

Scanning electron microscopy (SEM) micrographs, accompanied by electron-dispersive X-ray (EDX) spectra, were obtained using a Zeiss EVO LS15 microscope operated under high-vacuum conditions. A Miniflex600-PXRD instrument was used to produce Powder X-ray diffractograms (XRD). Optical Density (OD) measurements of the formazan product during the cell viability assays were performed using a BioTek uQuant Microplate spectrophotometer (BioTek® Instruments, Inc., Winooski, VT, USA) at 570 and 690 nm. Vanadium concentrations were measured in solution by inductively coupled plasma optical emission spectroscopy (ICP-OES), with the vanadium emission wavelength set at 290.88 nm.

Preparation of the polymer solutions

A 14-weight (wt.)% solution of PVA was prepared in ultrapure water by stirring and heating at 90 °C for 1 hour. Similarly, a 1 wt% solution of CS was prepared in 90% acetic acid by heating it at 45 °C for 3 hours, followed by 2 hours of sonication at the same temperature. A PVA : CS volume ratio of 7 : 3 was optimized. The complex-loaded polymeric solution was prepared by two methods. The direct blending (DB) method involved adding 10 mg of each vanadium compound (**1** or **2**) to the PVA-CS polymeric solution. In the solvent blending method (SB), 10 mg of each metal compound was dissolved in 1 mL of ethanol before adding it to the bulk polymeric solution. After adding the respective metal compounds, the resultant polymer solutions were stirred overnight at room temperature to achieve a homogeneous dispersion of each metal compound.

Fabrication of the vanadium compound-loaded electrospun nanofibers (ENFs)

The PVA-CS polymer solutions containing the metal compounds were each placed into a 5 mL plastic syringe and affixed onto a syringe pump of an Inovenso nanospinner 24 multinozzle electrospinning/spraying machine. The flat collector plate was covered with a 200 × 200 mm^2 piece of aluminium foil and locked into position 170 mm away from the electrospinning nozzle. The electrospinning process was set to operate at 35 kV and 1.5 mL h^{-1}. The electrospinning process was concluded once all the polymer solution from the syringe had been extruded and the resultant ENFs had accumulated on

the collector unit. The morphological features of the ENFs were investigated using ImageJ.[22]

In vitro release study

The metal-based drug release profiles from the PVA-CS ENF framework were evaluated using a pH-dependent method at controlled physiological temperature conditions (37 °C). The rationale is that, after oral administration, a metallopharmaceutical must retain structural integrity in the extremely acidic conditions of stomach acid and be resistant to enzymatic degradation.[23] For the first 2 hours, 5 mg of each vanadium complex-ENF conjugate was placed in a hydrochloric acid solution of pH 2.16 to simulate the stomach pH (1 – 3). Secondly, Tris–HCl was added dropwise to adjust the pH to 7.2 to simulate gastrointestinal tract conditions, and the aliquot solutions were digested for an additional 3 hours. During each pH test, the metal-based drug concentrations released were measured by UV-Vis spectrophotometry every 15 minutes, at 306 nm for **1** and 324 nm for **2**.

The determination of the total amount of metal complex loaded on each ENF sample was adapted from a literature method.[24] This involved the complete dissolution of the ENF (5 mg) in a solvent of low pH (0.1 M HCl) and measuring the UV-Vis spectrum of the solution. The concentration was then calculated using the molar extinction coefficient (ε_{max}), previously determined for each complex using the Beer–Lambert law at known concentrations.

Drug loading percentage and entrapment efficacy

The drug loading percentage was determined from the experiment used to calculate the total amount of metal complex loaded in each metal complex-ENF hybrid, as described under dissolution testing. The following equation was used:

$$\mathrm{DL}(\%) = \frac{W_{\mathrm{UV}}}{W_{\mathrm{MAT}}} \times 100 \quad (1)$$

where W_{UV} is the total mass of the metal compound within the PVA-CS ENF matrix, and W_{MAT} is the mass of the ENF dissolved (5 mg).

The drug entrapment efficacy of each metal complex-polymeric nanocomposite was calculated by:

$$\mathrm{EE}(\%) = \frac{W_{\mathrm{UV}}}{W_{\mathrm{ES}}} \times 100 \quad (2)$$

where W_{ES} is the amount of a vanadium compound dissolved before the electrospinning procedure.[24]

Antioxidant activity

The antioxidant activities of the individual ENFs nanohybrids and the free vanadium compounds towards the neutralization of the 2,2-diphenyl-1-picrylhydrazyl (DPPH) radical scavenging assay, as described in the literature.[25] An amount of 5 mg for each ENF was dissolved in 2 mL of ethanol in a test tube. For the free metal compounds, 2 mL of ethanolic 40 μM solutions was used. Thereafter, 2 mL of DPPH solution was added, and the test tubes and incubated in the dark for 1 hour. The solutions were then centrifuged, and absorbance at 517 nm was measured using UV-Vis spectrophotometry. The percentage (%) antioxidant activity was calculated using:

$$\%\ \text{Antioxidant activity} = \left[\frac{(A_{\mathrm{C}} - A_{\mathrm{S}})}{A_{\mathrm{s}}}\right] \times 100 \quad (3)$$

where A_c is the absorbance of the control (DPPH), and A_S is the absorbance of the sample.

Cell line culturing

HepG2 liver, C2C12 skeletal muscle, and Caco-2 cell lines were purchased from Cellonex, South Africa. The cells were grown in culture flasks that contained Dulbecco's Modified Eagle Medium (DMEM) mixed with 20% fetal bovine serum, 4.0 mM l-glutamine, and sodium pyruvate, with the addition of 1 mL penicillin/streptomycin. The cells were incubated in an incubator (RS Biotech Galaxy, Irvine, UK) that maintained a humidified atmosphere of 5% CO_2 at 37 °C during cell growth. The cell media was changed every 2 to 3 days. The cells were subcultured when 80% confluency was achieved.

Cell viability and *in vitro* glucose metabolism studies

Cell viability was evaluated in HepG2 liver and C2C12 skeletal muscle cell lines to determine the cytotoxic effects of the vanadium complexes and the vanadium-loaded ENFs released from the ENF matrix over time. The analysis employed the 3-(4,5-dimethylthiazol-2-yl)-2,5-diphenyltetrazolium bromide (MTT) assay described by Kamiloglu *et al.*[26] cells were trypsinised into 96-well plates at a seeding density of 1.8×10^4 cells per well. Cells were then incubated for 24 hours to enable attachment and growth to semi-confluency. Thereafter, the cells were incubated with metal complexes and the complex-loaded ENFs at three doses (12.5, 25, and 50 μmol L^{-1}) at 37 °C for 24 and 48 hours, respectively. The media used for treatment was then discarded after re-immersion of the cells in 20 μL MTT salt solution (5 mg MTT in 1 mL 0.1 M PBS) and 100 μL culture media. Cell incubation was allowed for 4 h to permit the formation of blue formazan crystals. DMSO (100 μL/well) was then used to replace the MTT solution, and the plate was incubated for 1 hour at 37 °C. The optical density measurements were then recorded, and the percentage cell viability was calculated as follows:

$$\text{Cell viability}\ (\%) = \frac{\text{Average OD of treated cells}}{\text{Average OD of control cells}} \times 100 \quad (4)$$

A well-established cell culture protocol was used to assess glucose utilization as described by Valley *et al.*, with slight modifications.[27] 24-well plastic plates were used to seed the cells at a density of 6×10^5 cells·cm^{-2} and thereafter incubated for 24 hours to allow attachment. The incubation medium was then discarded, and the cells were incubated with vanadium complexes and the complex-loaded ENFS at three doses (12.5, 25, and 50 μmol L^{-1}) at 37 °C for 24 and 48 hours, respectively. Thereafter, cells were collected for glucose concentration measurement.

Intracellular uptake studies

A published method was used to evaluate the pattern of intracellular uptake of the inorganic component leached from each metal-loaded ENF.[28] 6-well plastic plates were used to seed the Caco-2 cells at a cell density of 6×10^5 cells·cm^{-2}. 24 hours before the experiments, fresh culture medium was added. After removal of the incubation medium, a metal-loaded ENF dose of 12.5 μmol L^{-1} was added to the medium for varying times (1–48 hours). When the incubation periods were complete, cells were washed three times with PBS and lysed with 0.5 mL sub-boiled HNO_3 per well for 1 hour at room temperature. The vanadium concentration was then quantified using ICP-OES. The samples were diluted to 5 mL prior to this analysis, and the instrument was calibrated at 311 nm, see Fig. S1.

Results and discussion

Morphology

The morphologies of the ENFs were analyzed using SEM-EDX, and their average diameters are presented as related ENF diameter distribution histograms. In terms of the unmodified PVA|CS-ENFs, Fig. S2 shows that the ENFs were smooth with minimal bead formation, whilst the vanadium complex-loaded ENFs (Fig. 2 and S3–S5) appear to have fewer imperfections in the SEM micrographs of PVA|CS-**1** (DB)-ENFs (Fig. 2) and PVA|CS-**1** (SB)-ENFs (Fig. S2). The ENF diameter distribution for the unmodified PVA|CS ENFs was determined to be between 50 and 500 nm, with an average diameter of 235.8 nm (Fig. S2).

A comparative analysis was made of the average diameters of unmodified ENFs and those of ENFs loaded with different vanadium compounds. More specifically, the ENFs prepared by the DB method exhibited smaller diameter distributions than the neat ENF. This cross-sectional narrowing of the modified ENFs is ascribed to the enhanced conductivities of the individual vanadium compound polymer bulk solutions experienced during electrospinning. In turn, faster polymer extrusion from the spinneret led to thinner ENFs deposited on the collector unit.[29,30]

Contrastingly, the ENFs prepared by the SB method produced larger diameter distributions and average diameters. This can be attributed to the presence of ethanol in the solvent system of the different bulk polymeric solutions, where the alcoholic medium decreases the dielectric constant and volatility of the mixed solvent system. Subsequently, polymer ejection from the spinneret is retarded, resulting in larger average diameters.[31]

Characterization

Elemental mapping using SEM-EDX (Fig. 3 and S6–S8) was used to verify the presence of the metal complexes in the fabricated ENFs. The results show uniform dispersion of C, N, O, and V across the specific regions of analysis, confirming that the different vanadium complexes were incorporated into their corresponding ENFs. Interestingly, the ENFs prepared by the DB method contain a higher percentage of vanadium than those prepared by the SB method, indicating a higher loading capacity of vanadium complexes for the former method.

Although several factors can influence the drug-loading efficacy of ENFs, in this study, the only difference between the techniques was the use of ethanol in the SB method. Thus, the discrepancy in the drug loading capacities is accounted for by the greater solubility of the metal complexes in the mixed solvent system of the DB preparation (water and acetic acid), rather than the mixed solvent system employed during the SB preparation method, which contained ethanol as well as water and acetic acid.[32]

Structural analysis of the unmodified PVA|CS-ENFs and their metal complex-loaded ENFs was analyzed by FTIR spectroscopy (Fig. 4 and S9–S11). The different FTIR spectra of the metal complex-loaded ENFs showed characteristic IR bands related to the analogous vibrational stretches of the parent metal compounds. Indicatively, this infrared spectral analysis substantiates the inclusion of the metal compounds in the nano-structural polymeric matrix.

Furthermore, broad vibrational bands near 3300 cm^{-1} can be readily ascribed to the O–H and N–H groups of PVA and CS. In the vicinity of 2920 cm^{-1}, signals correspond to the stretching of the alkyl groups in PVA, while the band at 1716 cm^{-1} can be assigned to the carboxylic acid group of the crosslinking agent, acetic acid. The symmetric deformation of the NH_3^+

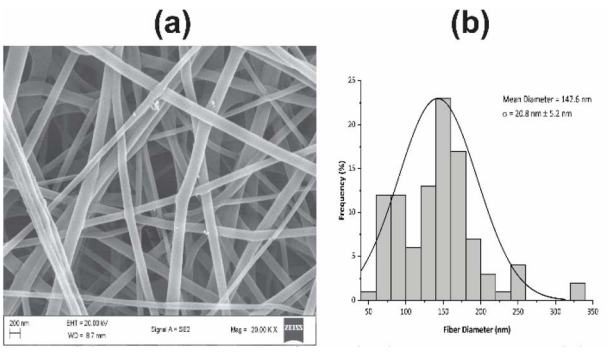

Fig. 2 (a) SEM image of PVA|CS-**1** (DB) ENFs and their (b) ENF diameter distribution histogram.

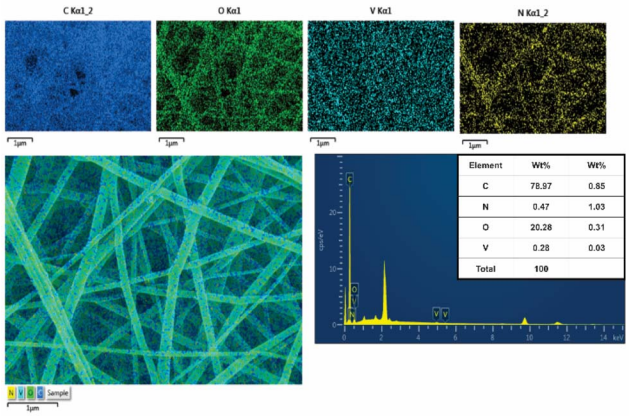

Fig. 3 Elemental mapping of PVA|CS-**1** (DB) ENFs.

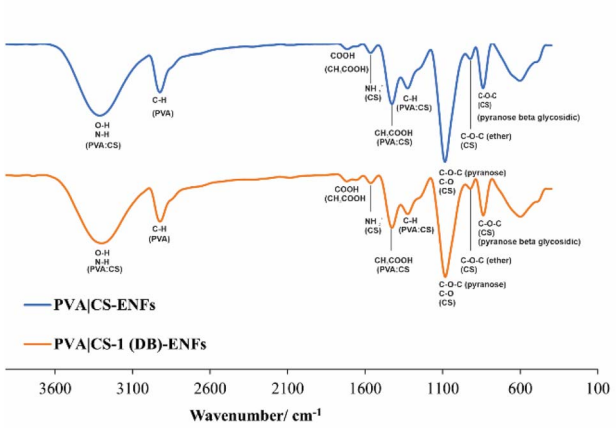

Fig. 4 Stacked FTIR spectra of PVA|CS-ENFs and PVA|CS-**1** (DB)-ENFs.

group of CS was induced by ionization of its primary amines in acidic media accounts which resulted in a low-intensity band at 1565 cm^{-1}, whilst the band at 1428 cm^{-1} is associated with the carboxylic acid groups of PVA and CS.

Furthermore, the FTIR stretch at 1329 cm^{-1} corresponds to C–H vibrations of PVA and CS, whereas the stretching frequencies in the range of 1086 – 840 cm^{-1} can be attributed to a skeletal vibration, which is related to a C–O stretch of the C–O–C glycoside ring in CS.[33] The vibrational bands of the metal complex-loaded ENFs are mostly the same due to the polymer being present in bulk, but a clear reduction in the intensities with shifts to lower wavenumbers can be related to the inclusion of the metal complexes into the PVA|CS nanocomposites.[34]

Powder X-ray diffraction is a versatile technique for studying the structural features of nanocomposites. Their overlay powder XRD patterns of the pure polymeric ENFs and their loaded ENFs are shown in Fig. 5 and S12. CS typically has three characteristic peaks in its XRD pattern (2Θ ~10.5°, 2Θ ~15.4°, and 2Θ ~20.1°), and PVA has two characteristic peaks (2Θ ~19.65° and 2Θ ~41.15°). Literature has shown that peaks for CS become weak until they eventually disappear with increasing amounts of PVA in the polymeric blend of PVA|CS.[21,35]

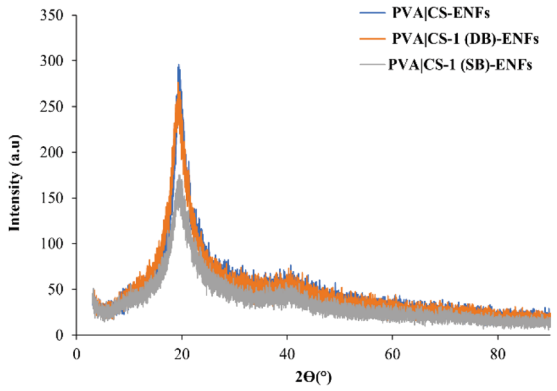

Fig. 5 Overlay powder XRD patterns of PVA|CS-ENFs and its ENFs loaded with **1**.

Thus, from the powder XRD patterns of the polymeric ENFs, only two peaks (2Θ = 19.61° and 2Θ = 40.28°) were observed, which are attributed to the crystalline nature of PVA, as it is present at a higher concentration in the blend. Broadening and significant decreases in the intensities of the distinctive peaks are observed upon addition of the metal complexes, confirming successful loading of the complexes into the polymer. These results show that the addition of the metal complexes increases the amorphous nature of the host polymer (PVA|CS), giving the prepared ENFs a semi-crystalline nature. Furthermore, these spectral changes are most evident with the peak at 40.28°, which can be accounted for by the weakening of intermolecular force and hydrogen bond disruption of the host polymer by the metal complexes.[35]

In vitro release studies

Studying drug release using a pH change method is an important technique used in the design of oral delivery systems. Drugs usually pass through the stomach and are then excreted into the intestines, where most absorption occurs.[36] Therefore, the release profiles of the ENFs were examined in the simulated harsh acidic conditions of the stomach (pH 2.16) for two hours (fed state), followed by adjusting the pH to the simulated intestinal conditions (pH ~7.2) and monitoring the release for a further 3 hours. In the case of oral drugs, it is desirable to have a slower initial drug "burst" to prevent stomach-related side effects such as nausea, ulceration, or perforation.[37]

The release profile for ENFs of **1** (Fig. S13) shows that the DB-prepared ENFs show a significantly lower initial burst than the SB-prepared ENFs, whereas the release profile for ENFs of **2** (Fig. S14) shows that both have low and comparable initial bursts. Lower initial bursts are usually associated with more homogeneously dispersed metal compounds within the polymer.[38] After 2 hours (fed state) at gastric pH, between 38 – 45% of the metal compounds were liberated from the loaded ENFs. Therefore, the doses of the metal compounds that could be released in the intestinal region where active absorption is thought to occur upon gastric emptying would be between 55–62%. These results support the intended role of the ENFs as prospective gastrointestinal delivery systems for the regulated release of the vanadium complexes. Subsequently, the released metal complexes can be potentially absorbed by the epithelial tissues. Although the metal compound dosages released under acidic pH are higher than the preferred 10% initial burst, the UV-Vis spectra showed that the metal compounds undergo no changes in nature and are stable under these conditions. This suggests that the metal compounds remain active during gastric emptying into the intestinal region and serve as the loading dose for bioavailability and absorption.[39]

At intestinal pH (7.2), the ENFs exhibited slower, more controlled release of the compounds over 3 hours, with most of the metal compound from the PVA|CS-**2** (DB)-ENFs released (~96%). The other ENF nanoconjugate released lower percentages of the metal compounds in a controlled manner, with considerable quantities remaining after 3 hours within the PVA-CS ENFs framework. This points to a high possibility that their

release can be extended to timescales of over 8 hours, making them eminently suitable for sustained release candidate drug systems.[39] This is especially true for PVA|CS-**1** (DB)-ENFs, as it only releases 58% of **1** at pH 7.2 after 5 hours of the pH change experiment. The higher initial burst of PVA|CS-**1** (DB)-ENFs may be attributed to partial localization of the vanadium complex near the ENF surface, leading to a more rapid release into the diffusion medium. Although this may contribute to gastrointestinal stomach upset or toxicity due to the increased levels of free vanadium compound, this formulation subsequently exhibited sustained-release under the intestinal pH condition.[40]

These sustained-release profiles could be explained by drug-polymer compatibility, which is primarily dependent on the drug or compound's solubility in the polymer–solvent system. A compound is more fully dispersed and encapsulated in an ENF when it is more soluble, allowing it to be released more slowly in the release media.[41] The structure of **1** has a greater number of oxygen and nitrogen groups, which can form strong hydrogen bonds with the organic polar solvents and substances that make up the polymer–solvent system, and therefore the ENFs of **1** have the most sustained release profiles. In the case of PVA|CS-**2** (SB)-ENFs, the slower release profile stems from the use of ethanol during preparation of the metal complex-loaded polymer strands, which most likely increased the solubility of the metal compounds in the polymer–solvent system due to **2** having more oxygen and nitrogen groups.

Entrapment efficacies and drug loading percentages

The ENFs in general exhibited high entrapment efficacies (EE), with ENFs of **1** showing slightly higher EE. This could again be attributed to the solubility of **1** in the polymer–solvent system.[41] This is also seen for ENFs of **2**, which were prepared by the SB method, where ethanol was added to the polymer–solvent system to enhance the solubility of **2** and lead to a higher EE. The calculated drug loading percentages (% DL) were found to be between 0.90 – 0.96%, which was near the theoretical value of 0.1% (w/w) for the complex-loaded ENFs. In general, the data were consistent with high EE and DL percentages.[24] The relatively higher entrapment efficacies seen in the ENFs of **1** are consistent with better compound-polymer compatibility within the chosen polymer–solvent systems, which led to a more homogenous dispersion of the metal compound into the ENF framework and contributed to the better sustained-release profiles observed (Table 1).[41]

Table 1 Entrapment efficacies and drug loading percentages of the complex-loaded ENFs

	Entrapment efficacy (%)	Drug loading% (w/w)
PVA|CS-**1** (DB)-ENFs	97	0.96
PVA|CS-**1** (SB)-ENFs	98	0.94
PVA|CS-**2** (DB)-ENFs	80	0.96
PVA|CS-**2** (SB)-ENFs	83	0.90

Antioxidant activity

Reactive oxygen species (ROS) are produced in excess in various tissues of diabetic patients. These ROS play roles in the development of diseases and are associated with the progression of pancreatic β-cell dysfunction.[42,43] The free radical scavenging ability of vanadium species has been reported in streptozotocin-induced diabetic rats.[44] This incited the research study to be extended to exploring the radical scavenging activities of the metal complex-loaded ENFs (Fig. 6). The results show that the ENFs encompassing the different metal complexes showed higher radical scavenging activities compared to the free vanadium compounds. Previous studies suggest that increased surface area results in greater antioxidant/radical-scavenging activities of bioactive components.[45] Furthermore, the existence of active hydroxyl and amino groups in the chitosan and PVA polymer chains, which have hydrogen-donating capabilities, may additionally contribute to increased radical scavenging capabilities during the degradation of the polymeric framework of the ENFs upon the release of the vanadium complexes.[25,46]

Intracellular uptake studies

Effective translation of vanadium-based antidiabetic agents critically depends on their intestinal absorption, as poor gastrointestinal uptake has historically limited their therapeutic applicability despite strong *in vitro* insulin-mimetic activity.[4,17,47] In this study, ICP-OES analysis was performed as an initial investigative step to quantify vanadium trace concentrations following exposure to vanadium heterocyclic compound-loaded electrospun nanofibers (ENFs) in an intestinal cell line, thereby providing insight into the capacity of these formulations to facilitate vanadium absorption from the intestinal environment into downstream cellular systems, as shown in Table S1.[48,49] Crucially, these studies were designed to evaluate the absorption of the vanadium species released from the polymeric matrix of the ENFs, post gastrointestinal degradation.

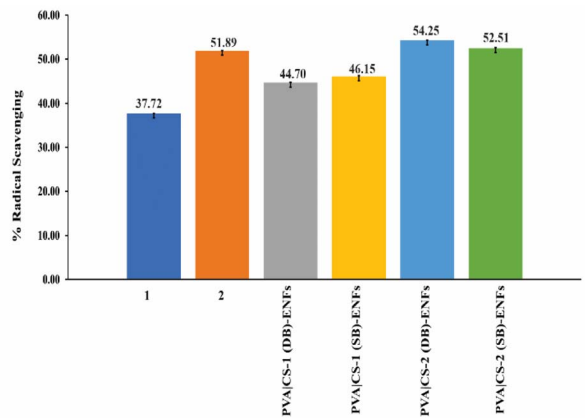

Fig. 6 Radical scavenging activities of the vanadium complex-loaded ENFs against their free metal complexes ($\sigma < 0.05$, $n = 3$).

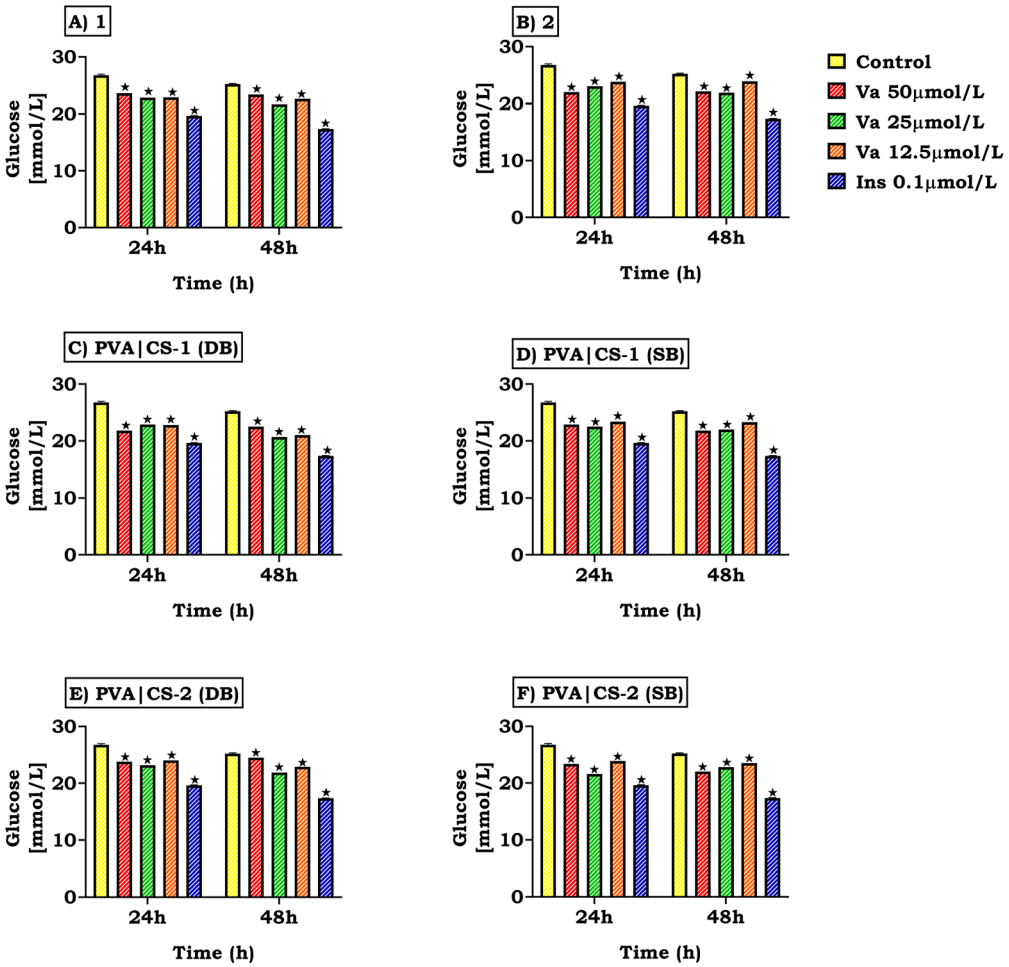

Fig. 7 The effects of vanadium heterocyclic compound-loaded ENFs on glucose uptake in HepG2 cell lines over the incubation period of 24 and 48 hours. $\sigma < 0.05$ in comparison to the control group (Va: concentration of complex or complex-loaded ENF, and Ins: insulin positive control).

The ICP-OES results revealed measurable, sustained vanadium concentrations across all formulations over time, with concentrations remaining relatively stable from early (1–4 hours) to prolonged (24–48 hours) time points. This temporal consistency suggests that the PVA-chitosan ENF matrix effectively modulates vanadium release, preventing rapid luminal loss while enabling gradual absorption across the intestinal barrier.[4] Importantly, both vanadium compound **1** and compound **2**-loaded ENFs demonstrated comparable absorption profiles irrespective of ligand coordination mode (DB *vs.* SB), indicating that polymer-mediated delivery plays a dominant role in governing intestinal bioavailability rather than ligand chemistry alone.

The absence of a pronounced burst release in the intestinal setting is particularly relevant, as excessive free vanadium ions in the gastrointestinal tract have been associated with mucosal irritation, oxidative stress, and poor systemic tolerance.[47,50,51] By maintaining vanadium concentrations within a narrow, controlled range, the ENF system can likely facilitate the safer translocation of vanadium species from the intestinal lumen to peripheral tissues, thereby establishing a prerequisite for downstream metabolic efficacy. These findings collectively support the hypothesis that electrospun polymeric matrices can overcome one of the principal limitations of vanadium pharmacology—namely, inefficient and erratic intestinal absorption.[52]

Cell viability and *in vitro* glucose metabolism studies

Having established that vanadium is effectively absorbed from the intestinal environment *via* the ENF formulations, subsequent evaluation of cytocompatibility in hepatic (HepG2) and skeletal muscle (C2C12) cells was essential to confirm that absorbed vanadium concentrations do not elicit cytotoxic effects. Across all tested doses (12.5–50 μg mL^{-1}) and exposure periods (24–48 h), none of the vanadium-loaded ENFs compromised cell viability relative to controls. This finding is notable given that intracellular accumulation of vanadium has previously been linked to mitochondrial dysfunction and apoptosis when administered in non-encapsulated forms.[47] This further suggests that the release behaviours observed for the compound-loaded ENFs, including the initial bursts, did not exhibit any detrimental biological complications within the investigated concentration range.

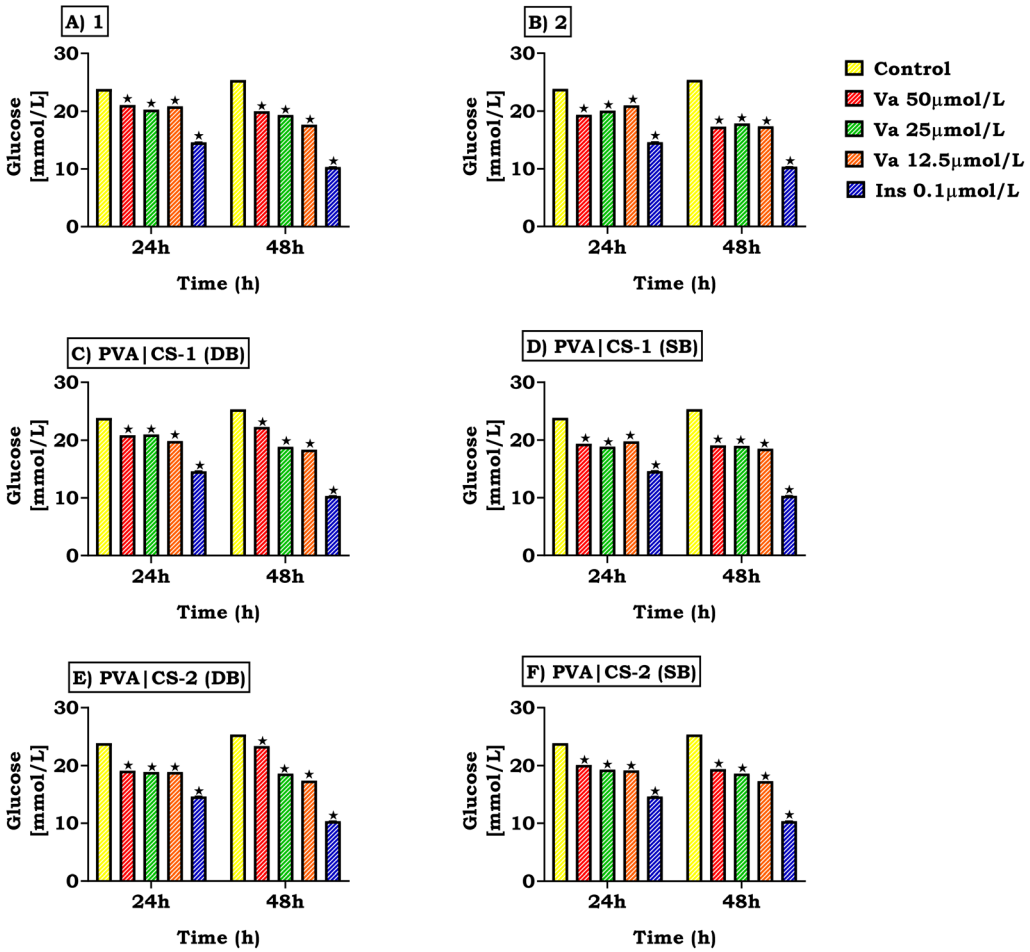

Fig. 8 The effects of vanadium heterocyclic compound-loaded ENFs on glucose uptake in C2C12 cell lines over the incubation period of 24 and 48 hours. $\sigma < 0.05$ in comparison to the control group (Va: concentration of complex or complex-loaded ENF, and Ins: insulin positive control).

The preservation of cell viability in both liver and muscle models suggests that intestinally absorbed vanadium delivered *via* ENFs remains within a therapeutically safe window upon reaching target cells, as shown in Fig. S15 and S16.[53–55] This supports the notion that controlled intestinal absorption and regulated cellular exposure are mechanistically linked, with polymer encapsulation reducing the likelihood of toxic intracellular vanadium spikes. Furthermore, the comparable cytocompatibility observed between DB and SB formulations reinforces earlier reports that ligand coordination primarily influences biological activity rather than toxicity when systemic exposure is appropriately regulated.

Following confirmation of both intestinal absorption and cellular safety, the functional metabolic consequences of vanadium delivery were assessed using glucose utilization assays in HepG2 and C2C12 cells (see Fig. 7 and 8). All vanadium heterocyclic compound-loaded ENFs significantly enhanced glucose uptake relative to untreated controls, demonstrating that intestinally absorbed vanadium species could remain biologically active upon reaching hepatic and skeletal muscle cells. This is consistent with the established insulin-mimetic behaviour of vanadium complexes, which act by inhibiting protein tyrosine phosphatases, activating PI3K/AKT signalling, and increasing the translocation of glucose transporters such as GLUT2 and GLUT4.[47,56]

Among the tested formulations, vanadium compound **1**-loaded ENFs consistently exhibited superior glucose-lowering effects in both cell lines compared to vanadium compound **2**-loaded ENF systems. This enhanced efficacy is likely attributable to ligand-dependent stabilization of bioactive vanadium species and to improved interactions with the insulin signalling machinery, as previously reported for benzimidazole-containing vanadium complexes.[14,55] Furthermore, the higher entrapment efficacy and release profile of the vanadium compound **1**-loaded ENFs can potentially increase bioavailability of **1** in the GI tract. The fact that these metabolic benefits were observed following confirmed intestinal absorption further strengthens the translational relevance of compound **1** as a lead candidate.

Interestingly, a clear dose–response relationship was not evident across the tested concentration range, with glucose utilization appearing to plateau at intermediate doses. This phenomenon has been widely documented in vanadium pharmacodynamics and is generally attributed to early saturation of

insulin–responsive pathways and transporter availability.[47] Moreover, sustained vanadium delivery from ENFs following intestinal absorption may promote prolonged pathway activation rather than acute, dose-dependent spikes, thereby favouring metabolic stability over maximal stimulation.

Conclusions

Nanohybrids of the optimized PVA|CS polymeric blend and the glucose-lowering vanadium benzimidazole compounds were fabricated *via* electrospinning. SEM morphological investigation of the free PVA|CS ENFs and the nanocomposites revealed that the latter have thinner average ENF diameters with no apparent imperfections. SEM elemental analysis shows that the metal complex-polymeric nanoconjugates exhibit elemental distribution throughout the nanostructural materials. The incorporation of the metal complexes into the ENF matrix was corroborated by solid-state FTIR spectroscopy and powder X-ray diffractometry. UV-Vis spectrophotometric measurements showed that the preparation methods of the polymer solution have a profound influence on the dissolution rates of the PVA|CS ENFs of **1** and **2**, respectively. Generally, the metal complexes are released faster from the polymeric matrices at lower concentrations in an acidic medium mimicking stomach conditions, whereas slower, elevated release was observed at pH 7.2, which simulates intestinal conditions. The high loading percentages of the respective metal compounds rendered complementary activities of the metal complex and the PVA|CS ENFs to radically scavenge the DPPH radical. The majority of the nanoconjugates exhibited controlled release kinetics, whereas PVA|CS-2 (DB)-ENFs showed rapid release of ~96% within 3 h. The cell line studies demonstrated a coherent mechanistic progression from controlled intestinal absorption of vanadium to preserved cellular viability, and ultimately to enhanced glucose utilization in key metabolic tissues. The integration of ICP-OES absorption data with cellular and functional outcomes underscores the critical role of electrospun nanofiber systems in overcoming longstanding limitations of vanadium-based therapeutics. Notably, vanadium compound **1**-loaded ENFs emerged as the most promising formulation, exhibiting favourable intestinal absorption, excellent cytocompatibility, and robust insulin-mimetic activity, thereby warranting further investigation in insulin-resistant and *in vivo* models. Collectively, the reproducible antioxidant, release, and cell-based results further corroborate that the vanadium compound-loaded ENFs allow for controlled release of the respective metal-based drugs from the polymer matrix.

Author contributions

Sanam Maikoo (SM): writing – original draft preparation, methodology, formal analysis, investigation, data curation, visualization, co-funding, co-supervision of MM. Mongezi Majebe (MM): methodology, investigation. Andile Kathi: writing – review & editing, resources. Allen Mambanda: writing – review & editing, methodology, co-host of SM. Bongeka Mshengu (BM): writing – original draft preparation, methodology, formal analysis, investigation, data curation, visualization. Phikelelani Ngubani: conceptualization, writing – review & editing, co-funding and resources, supervision of BM. Lindokuhle Patience Mabuza: conceptualization, writing – review & editing, co-funding, and resources. Irvin Noel Booysen: funding acquisition, conceptualization, writing – review & editing, methodology, main host of SM, co-funding and resources, supervision of MM.

Conflicts of interest

There are no conflicts to declare.

Data availability

Data is available from the corresponding upon reasonable request.

Acknowledgements

The authors are grateful for the financial assistance from the National Research Foundation of South Africa (NRF): Incentive funding for Rated Researchers (Grant No. 114737), NRF CPRR (Grant No. 120834), and the University of KwaZulu-Natal.

References

1 K. L. Ong, L. K. Stafford, S. A. McLaughlin and et. al., *Lancet*, 2023, **402**, 203–234.
2 B. Naidoo, S. Pillay and D. Wilson, *J. Endocrinol.*, 2024, **29**, 43–47.
3 V. Ugirinema, F. Odei-Addo, C. L. Frost and Z. R. Tshentu, *Molecules*, 2024, **29**, 724.
4 L. M. Amaral, T. Moniz, A. M. Silva and M. Rangel, *Int. J. Mol. Sci.*, 2023, **24**, 15675.
5 B. Homayun, X. Lin and H.-J. Choi, *Pharmaceutics*, 2019, **11**, 129.
6 S. Uppal, K. S. Italiya, D. Chitkara and A. Mittal, *Acta Biomater.*, 2018, **81**, 20–42.
7 S. S. Garg, R. Dey, A. Sharma and J. Gupta, *J. Drug Delivery Sci. Technol.*, 2024, **100**, 106119.
8 D. M. Cahyani, A. S. Mubarok, B. S. Hariawan, I. Amalina, P. Drake, T. Parumasivam, R. K. Sahu, M. A. S. Rijal, R. Sari and A. Miatmoko, *Braz. J. Med. Biol. Res.*, 2025, **58**, e14459.
9 M. Liu, R. Wang, M. P. M. Hoi, Y. Wang, S. Wang, G. Li, C. T. Vong and C.-M. Chong, *Int. J. Nanomed.*, 2025, 6221–6252.
10 H. Maleki, K. Khoshnevisan, S. M. Sajjadi-Jazi, H. Baharifar, M. Doostan, N. Khoshnevisan and F. Sharifi, *J. Nanobiotechnol.*, 2021, **19**, 1–34.
11 S. Kajdič, O. Planinšek, M. Gašperlin and P. Kocbek, *J. Drug Delivery Sci. Technol.*, 2019, **51**, 672–681.
12 S. Lian, D. Lamprou and M. Zhao, *Int. J. Pharm.*, 2024, **651**, 123641.
13 N. Xulu, P. Ngubane, A. Khathi, I. Booysen and N. Sibiya, *Diabetes, Metab. Syndr. Obes.: Targets Ther.*, 2021, 4321–4333.

14 B. Mbatha, A. Khathi, N. Sibiya, I. Booysen, P. Mangundu and P. Ngubane, *BioMetals*, 2021, **34**, 161–173.
15 S. Sibiya, B. Msibi, A. Khathi, N. Sibiya, I. Booysen and P. Ngubane, *Can. J. Physiol. Pharmacol.*, 2019, **97**, 1169–1175.
16 B. Mbatha, A. Khathi, N. Sibiya, I. Booysen, P. Mangundu and P. Ngubane, *Can. J. Physiol. Pharmacol.*, 2021, **99**, 402–410.
17 P. Mangundu, S. Maharaj, C. G. L. Veale and I. N. Booysen, *Polyhedron*, 2022, **223**, 115992.
18 Y. Cheng, B. Farasati Far, M. Jahanbakhshi, S. Bahrami, P. Tamimi, M. Sedaghat and E. Ghazizadeha, *RSC Adv.*, 2023, **13**, 18450–18460.
19 B. S. Alotaibi, A. K. Khan, Z. Kharaba, H. Yasin, R. Yasmin, M. Ijaz, M. Khan and G. Murtaza, *ACS Omega*, 2024, **9**, 12825–12834.
20 G. C. d. Mata, M. S. Morais, W. P. d. Oliveira and M. L. Aguiar, *Polymers*, 2022, **14**, 4856.
21 Y.-T. Jia, J. Gong, X.-H. Gu, H.-Y. Kim, J. Dong and X.-Y. Shen, *Carbohydr. Polym.*, 2007, **67**, 403–409.
22 C. A. Schneider, W. S. Rasband and K. W. Eliceiri, *Nat. Methods*, 2012, **9**, 671–675.
23 V. Friuli, S. Pisani, B. Conti, G. Bruni and L. Maggi, *Polymers*, 2022, **14**, 2127.
24 L. É. Uhljar, S. Y. Kan, N. Radacsi, V. Koutsos, P. Szabó-Révész and R. Ambrus, *Pharmaceutics*, 2021, **13**, 556.
25 M. Rostami, M. Ghorbani, M. Delavar, M. Tabibiazar and S. Ramezani, *Int. J. Biol. Macromol.*, 2019, **135**, 698–705.
26 S. Kamiloglu, G. Sari, T. Ozdal and E. Capanoglu, *Food Front.*, 2020, **1**, 332–349.
27 M. P. Valley, N. Karassina, N. Aoyama, C. Carlson, J. J. Cali and J. Vidugiriene, *Anal. Biochem.*, 2016, **505**, 43–50.
28 R. Himanshu, P. Jakir, H. Pradnya, P. Suneel and S. Rahul, *J. Drug Deliv. Therapeut.*, 2013, **3**, 20–29.
29 U. Aggarwal, A. K. Goyal and G. Rath, *Mater. Sci. Eng. C*, 2017, **75**, 125–132.
30 N. Amariei, L. Manea, A. Bertea, A. Bertea and A. Popa, *IOP Conf. Ser.: Mater. Sci. Eng.*, 2017, **209**, 012092.
31 Z. Song, S. W. Chiang, X. Chu, H. Du, J. Li, L. Gan, C. Xu, Y. Yao, Y. He and B. Li, *J. Appl. Polym. Sci.*, 2018, **135**, 45787.
32 A. Deepak, A. K. Goyal and G. Rath, *J. Drug Delivery Sci. Technol.*, 2018, **43**, 379–387.
33 D. M. Suflet, I. Popescu, I. M. Pelin, D. L. Ichim, O. M. Daraba, M. Constantin and G. Fundueanu, *Pharmaceutics*, 2021, **13**, 1461.
34 M. Ali and A. Gherissi, *Int. J. Mech. Eng.*, 2017, **17**, 15–28.
35 K. A. Abdalkarim, S. B. Aziz, R. T. Abdulwahid, S. M. Alshehri, T. Ahamad, J. M. Hadi and S. A. Hussein, *Arab. J. Chem.*, 2021, **14**, 103215.
36 M. K. Gaydhane, C. S. Sharma and S. Majumdar, *RSC Adv.*, 2023, **13**, 7312–7328.
37 I. Villegas, C. La Casa, C. A. de la Lastra, V. Motilva, J. M. Herrerıas and M. a. J. Martın, *Life Sci.*, 2004, **74**, 873–884.
38 S. Kalachandra, L. Dongming and S. Offenbacher, *J. Mater. Sci.: Mater. Med.*, 2002, **13**, 53–58.
39 U. E. Illangakoon, T. Nazir, G. R. Williams and N. P. Chatterton, *J. Pharm. Sci.*, 2014, **103**, 283–292.
40 A. Ścibior, Ł. Pietrzyk, Z. Plewa and A. Skiba, *J. Trace Elem. Med. Biol.*, 2020, **61**, 126508.
41 S.-F. Chou, D. Carson and K. A. Woodrow, *J. Controlled Release*, 2015, **220**, 584–591.
42 H. Kaneto, N. Katakami, M. Matsuhisa and T.-a. Matsuoka, *Mediat. Inflamm.*, 2010, **2010**, 453892.
43 M. Mihailović, S. Dinić, J. Arambašić Jovanović, A. Uskoković, N. Grdović and M. Vidaković, *Antioxidants*, 2021, **10**, 480.
44 U. Ashiq, R. A. Jamal, M. Mahroof-Tahir, Z. T. Maqsood, K. M. Khan, I. Omer and M. I. Choudhary, *J. Enzyme Inhib. Med. Chem.*, 2009, **24**, 1336–1343.
45 A. R. Neves, M. Lúcio, S. Martins, J. L. C. Lima and S. Reis, *Int. J. Nanomed.*, 2013, **8**, 177–187.
46 M. Curcio, F. Puoci, F. Iemma, O. I. Parisi, G. Cirillo, U. G. Spizzirri and N. Picci, *J. Agric. Food Chem.*, 2009, **57**, 5933–5938.
47 D. Rehder, *Metallomics*, 2015, **7**, 730–742.
48 A. Andreadi, P. Lodeserto, F. Todaro, M. Meloni, M. Romano, A. Minasi, A. Bellia and D. Lauro, *Int. J. Mol. Sci.*, 2024, **25**, 7028.
49 Y. V. Simos, K. Spyrou, M. Patila, N. Karouta, H. Stamatis, D. Gournis, E. Dounousi and D. Peschos, *Asian J. Pharm. Sci.*, 2021, **16**, 62–76.
50 K. H. Thompson and C. Orvig, *J. Inorg. Biochem.*, 2006, **100**, 1925–1935.
51 K. H. Thompson, J. Lichter, C. LeBel, M. C. Scaife, J. H. McNeill and C. Orvig, *J. Inorg. Biochem.*, 2009, **103**, 554–558.
52 B. P. Panda, M. X. Wei, N. K. H. Shivashekaregowda and S. Patnaik, *Proceedings*, 2021, **78**, 14.
53 D. M. Makanyane, L. P. Mabuza, P. Ngubane, A. Khathi, A. Mambanda and I. N. Booysen, *ChemMedChem*, 2024, **19**, e202400477.
54 D. M. Makanyane, S. Maikoo, F. R. Van Heerden, L. Rhyman, P. Ramasami, L. P. Mabuza, P. Ngubane, A. Khathi, A. Mambanda and I. N. Booysen, *J. Inorg. Biochem.*, 2024, **255**, 112541.
55 B. Mbatha, A. Khathi, N. Sibiya, I. Booysen and P. Ngubane, *Evidence-Based Complementary Altern. Med.*, 2022, **2022**, 5372103.
56 R. A. DeFronzo, E. Ferrannini, L. Groop, R. R. Henry, W. H. Herman, J. J. Holst, F. B. Hu, C. R. Kahn, I. Raz and G. I. Shulman, *Nat. Rev. Dis. Primers*, 2015, **1**, 15019.